IEEE Access
Multidisciplinary | Rapid Review | Open Access Journal

Received August 22, 2019, accepted September 17, 2019, date of publication September 20, 2019, date of current version October 2, 2019.

Digital Object Identifier 10.1109/ACCESS.2019.2942526

Position Tracking Control of Tailsitter VTOL UAV With Bounded Thrust-Vectoring Propulsion System

LINFENG WU, HUANYU LI, YINGJIE LI, AND CHUNWEN LI
Department of Automation, Tsinghua University, Beijing 100084, China

Corresponding author: Linfeng Wu (wulf13@mails.tsinghua.edu.cn)

This work was supported by the National Basic Research Program of China (973 Program).

ABSTRACT This paper presents an adaptive position tracking controller for a special kind of tailsitter vertical take-off and landing (VTOL) unmanned aerial vehicle (UAV). The distinctive part of this VTOL aircraft is its thrust-vectoring propulsion system, which allows the aircraft to achieve long-range flight at high-efficiency. However, there are two main problems encountered in the control design for this aircraft in vertical mode. One problem is that the mass and inertia tensor are unknown parameters because of the fuel consumption. The other problem is that the thrust vector is bounded both in amplitude and orientation, leading to the boundedness of control input. In this paper, we use a complementary filter to estimate the mass and an adaptive law to compensate the error caused by inertia uncertainty. A Lyapunov-based control law with nested saturation function is proposed to solve the problem of input boundedness. Finally, the global asymptotic stability is proven for the simplified model and the effectiveness is illustrated through simulation.

INDEX TERMS Tailsitter UAV, vectoring thrust, position tracking control.

I. INTRODUCTION

Over the past few years, the tailsitter airframe has received increasing interest because of its unique advantages over the typical fixed-wing aircraft and hovercraft. Fixed-wing aircrafts are generally less expensive and more energy efficient since they do not require any additional propulsion system to take off and land, but instead, they require a suitable runway and cannot hover to interact with stationary objects. On the other hand, hovercrafts are able to hover at an arbitrarily low speed, as well as take off and land in confined areas, but their speed in horizontal cruise mode is too low to achieve long-range flight. Tailsitter aircraft combines the benefits of fixed-wing aircraft and hovercraft: it can take off and land on its tail without any additional propulsion system, and convert the mode from vertical flight to horizontal flight to achieve long-range flight as efficiently as the typical fixed-wing aircraft can do [1].

Many researchers have made great contributions to the study of the tailsitter airframe. The authors in [2] designed a T-wing tailsitter UAV, which uses propeller wash over its wing and fin control surfaces to effect control during hover flight. They first achieved the hovering control and then implemented the transition flight test successfully. In [3], a ITU-BYU tailsitter equipped with a hybrid propeller-ducted fan propulsion system has been designed as a trade-off approach between speed and power limitation. A canard-main wing-shroud propeller configuration for tailsitter was proposed and nice experimental results were presented in [4], [5]. The researchers in [6] designed a quadcopter tailsitter called VertiKUL which did not rely on control surfaces. However, most of the tailsitter aircrafts in previous studies are made with propellers or duct fans, which had low thrust and less efficiency. As a result, the cruise speed and flight range of such aircrafts are unsatisfactory.

To solve this problem, we designed a tailsitter aircraft controlled by a thrust-vectoring propulsion system, which is composed of 2 turbojet engines and 2 vectored nozzles, with the capacity of providing high-amplitude vectoring thrust, thus achieving a higher cruise speed and a larger flight range than those tailsitter aircrafts using propellers or duct fans [7]. There is no additional propulsion system required for our aircraft in the vertical flight mode, which reduces the dead-weight and improves energy efficiency for the horizontal flight. However, such a configuration also brings some difficulties in control design. First, when the tailsitter aircarft

The associate editor coordinating the review of this manuscript and approving it for publication was Xudong Zhao.

is hovering at a relatively low speed, the control surfaces become invalid and the vectoring thrust bounded both in amplitude and orientation becomes the only control input, leading to the boundedness of translational thrust and rotational torque. Second, the mass and inertia tensor of aircraft are time-varying due to the consumption of aviation fuel by the turbojet engines. Besides, an undesirable rolling torque is brought in by the turbines at different rotation speed. Last but not least, the inherent coupling between translation and rotation leads to the non-minimum phase property in the dynamics of the tailsitter aircraft.

In this paper, an adaptive position tracking controller based on nested saturation function is proposed for our tailsitter VTOL UAV with the thrust-vectoring propulsion system. The problems of input boundedness, parameter uncertainty and undesired torque are addressed to a certain extent. Boundedness of control input is a common problem on VTOL control and has been explored in many studies [8]–[12], but it is difficult to prove global asymptotic stability when both input boundedness and parameter uncertainty are taken into consideration [13]. One of the main problems is that in the presence of mass uncertainty, some derivatives are unavailable to caculate the desired torque input. The authors in [14] used command filter to bypass this problem. However, to achieve asymptotic stability, this command filter technique requires filter parameters to be arbitrarily large, which violates the boundedness of control torque. To solve this problem, we use the explicit complementary filter based on low-priced sensors to estimate mass and then regard it as a known constant in the stability analysis. The nested saturation function is one of the most powerful instrument to solve the global stabilization problem for a chain of integrators with input boundedness and bounded disturbances [15]. In our control design, a simple version of the nested saturation function approach is developed based on the work in [16], and the upper bound of control torque is derived. The attitude control of VTOL aircraft has been extensively studied and various nonlinear control approaches have been developed to deal with the input boundedness problem in the presence of parameter uncertainty and external disturbances [17]–[19]. We adopt the variable structure control algorithm introduced in [20], [21] to track the desired attitude in the presence of unknown inertia tensor and undesirable torque. The coupling between subsystem dynamics is still an open problem. Some previous work considers the coupling as an unknow disturbances [22], [23], while some choose to ignore it [24]. Considering the cascaded nature of the system, we use the intermediary control input and the quaternion extraction algorithm designed in [25] as a link between translational and rotational dynamics. Quaternion attitude representation is adopted to eliminate the singularities and reduce computational complexity [26]–[28]. The global asymptotic stability is proven and simulation results illustrate the effectiveness of our control method.

The rest of this paper is organized as follows. Section II introduces the dynamic model for the tailsitter aircraft equipped with the thrust-vectoring propulsion system. Section III describes the control law and the stability is proven in Section IV. Simulation results are presented in Section V and conclusions are drawn in Section VI.

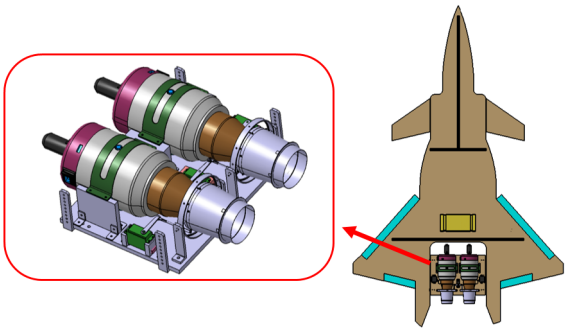

FIGURE 1. Tailsitter aircraft with thrust-vectoring propulsion system.

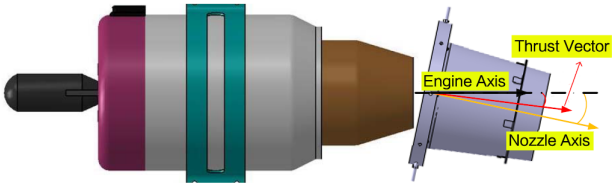

FIGURE 2. Turbojet engine with vectoring nozzle.

II. SYSTEM MODEL AND PROBLEM FORMULATION

In this section, we expound the mathematical model of our tailsitter aircraft and point out the problems caused by the thrust-vectoring propulsion system. Some assumptions are made to simplify the model.

A. PROPULSION SYSTEM

For the sake of guaranteeing VTOL aircraft to achieve position tracking, the propulsion system should be able to provide translational acceleration, roll torque, pitch torque and yaw torque. At least two thrust vectors are required to fulfill the requirement. In this paper, we focus on a simple but efficient propulsion system, which is presented in Fig. 1.

This propulsion system is composed of 2 turbojet engines and 2 vectoring nozzles. Turbojet engines are installed on the aircraft's tail and the engine axis is parallel to the longitudinal axis of aircraft's body. The rotation directions of two turbines are opposite, so the undesired rolling torques caused by two engines can be countered partly. The axis-symmetry nozzles are controlled by 3 steers to achieve pitch and yaw movement. By changing the axial direction of nozzles, the direction of airstream is influenced, thus changing the direction of thrust. Each pair of an engine and a nozzle could generate one independent thrust vector. Specific configuration is shown in Fig. 2 and 3.

This configuration, which is easy to implement, fulfills the requirements of propulsion system for position tracking. However, due to the limited capacity of turbojet engines and the limited range of steers, the thrust vectors, as control inputs

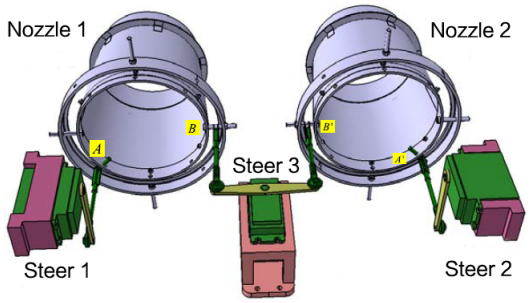

FIGURE 3. Vectoring nozzles controlled by steers.

for the aircraft dynamics, are bounded both in amplitude and orientation.

B. DYNAMIC MODEL

The tailsitter aircraft model is considered as a rigid body in this paper. Let the inertial frame and the body-fixed frame of the vehicle be denoted by $\mathcal{F}_i \triangleq \{\hat{\boldsymbol{e}}_1, \hat{\boldsymbol{e}}_2, \hat{\boldsymbol{e}}_3\}$ and $\mathcal{F}_b \triangleq \{\hat{\boldsymbol{e}}_{1b}, \hat{\boldsymbol{e}}_{2b}, \hat{\boldsymbol{e}}_{3b}\}$ respectively.

Let $\boldsymbol{p} \in \mathbb{R}^3$ and $\boldsymbol{v} \in \mathbb{R}^3$ denote the aircraft's position and linear velocity expressed in $\mathcal{F}_i$ respectively, and let $\boldsymbol{\omega} \in \mathbb{R}^3$ denote the angular velocity expressed in $\mathcal{F}_b$. The attitude of the aircraft is represented by the unit quaternion $\boldsymbol{Q} \triangleq (\eta, \boldsymbol{q}^T)^T$, where $\eta \in \mathbb{R}$, a scalar component, and $\boldsymbol{q} \in \mathbb{R}^3$, a three-element vector component, satisfy the unity constraint: $\eta^2 + \boldsymbol{q}^T\boldsymbol{q} = 1$. Rotation matrix $\boldsymbol{R}(\boldsymbol{Q}) \in \mathrm{SO}(3)$ denotes the map from inertial frame $\mathcal{F}_i$ to body-fixed frame $\mathcal{F}_b$, and is related to the unit-quaternion $\boldsymbol{Q}$ through the Rodriguez formula: $\boldsymbol{R}(\boldsymbol{Q}) = (\eta^2 - \boldsymbol{q}^T\boldsymbol{q})\boldsymbol{I}_3 + 2\boldsymbol{q}^T\boldsymbol{q} - 2\eta\boldsymbol{S}(\boldsymbol{q})$, where $\boldsymbol{I}_3$ is the 3-by-3 identity matrix and $\boldsymbol{S}(\cdot)$ is the cross product in matrix form. Specifically, for any given vector $\boldsymbol{v}_1 = (v_1, v_2, v_3)^T$ and $\boldsymbol{v}_2$, $\boldsymbol{S}(\boldsymbol{v}_1)$ satisfies the following equations:

$$\boldsymbol{S}(\boldsymbol{v}_1) = \begin{pmatrix} 0 & -v_3 & v_2 \\ v_3 & 0 & -v_1 \\ -v_2 & v_1 & 0 \end{pmatrix},$$
$$\boldsymbol{S}(\boldsymbol{v}_1)\boldsymbol{v}_2 = \boldsymbol{v}_1 \times \boldsymbol{v}_2.$$

The inverse of a unit quaternion is defined by $\boldsymbol{Q}^{-1} = (\eta, -\boldsymbol{q}^T)^T$ and the identity quaternion is $(1, 0, 0, 0)^T$. The multiplication between unit quaternion $\boldsymbol{Q}_1 = (\eta_1, \boldsymbol{q}_1^T)^T$ and $\boldsymbol{Q}_2 = (\eta_2, \boldsymbol{q}_2^T)^T$ is defined by $\boldsymbol{Q}_1 \odot \boldsymbol{Q}_2 = \left(\left(\eta_1\boldsymbol{q}_2 + \eta_2\boldsymbol{q}_1 + \boldsymbol{S}(\boldsymbol{q}_1)\boldsymbol{q}_2\right)^T, \eta_1\eta_2 - \boldsymbol{q}_1^T\boldsymbol{q}_2\right)^T$.

Let $\boldsymbol{T}_l \triangleq (T_{l1}, T_{l2}, T_{l3})^T$, $\boldsymbol{T}_r \triangleq (T_{r1}, T_{r2}, T_{r3})^T$ denote the thrust vectors which are expressed in $\mathcal{F}_b$ and generated by the left and right engines respectively as shown in Fig. 4, and let $\boldsymbol{T} = \boldsymbol{T}_l + \boldsymbol{T}_r \triangleq (T_1, T_2, T_3)^T$ denote the resultant thrust vector. Let the vectors from the center of gravity (CG) of the aircraft to the bearing points of $\boldsymbol{T}_r$ and $\boldsymbol{T}_l$ be denoted by $\boldsymbol{e}_r \triangleq (a_1, a_2, a_3)^T$ and $\boldsymbol{e}_l \triangleq (b_1, b_2, b_3)^T$, which are also expressed in $\mathcal{F}_b$. To simplify the relationship between thrust and torque, the following assumption is made:

Assumption 1: Two engines are installed symmetrically with the longitudinal axis of the aircraft. The CG of our aircraft and the bearing points of $\boldsymbol{T}_r$ and $\boldsymbol{T}_l$ are within the same plane normal to $\hat{\boldsymbol{e}}_{1b}$. Therefore we obtain $a_1 = b_1 = 0$, $a_2 = -b_2 > 0$, $a_3 = b_3 > 0$.

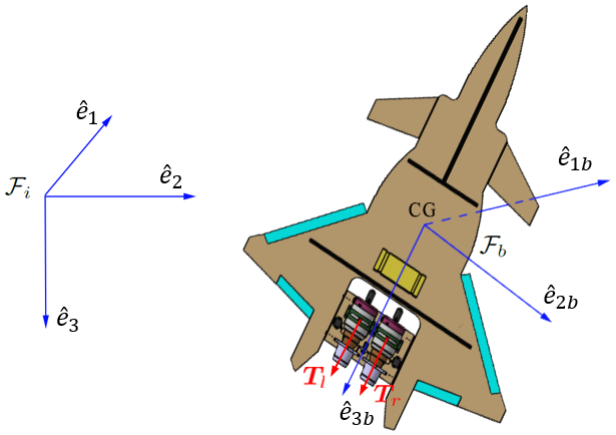

FIGURE 4. Inertial frame and body-fixed frame.

The tailsitter VTOL airframe with such a propulsion system can be modeled as:

$$\begin{cases} \dot{\boldsymbol{p}} = \boldsymbol{v}, \\ \dot{\boldsymbol{v}} = g\hat{\boldsymbol{e}}_3 - \dfrac{1}{m}\boldsymbol{R}(\boldsymbol{Q})^T\boldsymbol{T}, \\ \dot{\boldsymbol{Q}} = \dfrac{1}{2}\begin{pmatrix} -\boldsymbol{q}^T \\ \eta\boldsymbol{I}_3 + \boldsymbol{S}(\boldsymbol{q}) \end{pmatrix}\boldsymbol{\omega}, \\ \boldsymbol{I}_f\dot{\boldsymbol{\omega}} = \boldsymbol{\tau} - \boldsymbol{S}(\boldsymbol{\omega})\boldsymbol{I}_f\boldsymbol{\omega}, \end{cases}$$

where g is the gravitational acceleration, m is the mass of the aircraft, and $\boldsymbol{I}_f$ is the inertia tensor expressed in $\mathcal{F}_b$. Let L_{T0} denote the undesired rolling torque caused by the rotation of turbines. Under *Assumption* 1 the torque $\boldsymbol{\tau}$ can be formulated as:

$$\begin{aligned} \boldsymbol{\tau} &= \boldsymbol{e}_r \times (-\boldsymbol{T}_r) + \boldsymbol{e}_l \times (-\boldsymbol{T}_l) + (0, 0, L_{T0})^T \\ &= \begin{pmatrix} (T_{l2} + T_{r2})a_3 + (T_{l3} - T_{r3})a_2 \\ -(T_{l1} + T_{r1})a_3 \\ (-T_{l1} + T_{r1})a_2 + L_{T0} \end{pmatrix}. \end{aligned}$$

Define $\boldsymbol{z} \triangleq ((T_{l3} - T_{r3})a_2, 0, L_{T0})^T$ and $\boldsymbol{\tau}_u \triangleq ((T_{l2} + T_{r2})a_3, -(T_{l1} + T_{r1})a_3, (-T_{l1} + T_{r1})a_2)^T$, then we obtain

$$\begin{aligned} \boldsymbol{\tau} &= \boldsymbol{\tau}_u + \boldsymbol{z}, \\ \boldsymbol{T} &= T_3\hat{\boldsymbol{e}}_3 + \frac{1}{a_3}\boldsymbol{S}(\hat{\boldsymbol{e}}_3)\boldsymbol{\tau}_u. \end{aligned} \tag{1}$$

Although $\boldsymbol{z}$ is unknown, it should be noted that in hover mode, the longitudinal thrust is much larger than the lateral thrust, which means $T_{l3} \approx \|\boldsymbol{T}_l\|$ and $T_{r3} \approx \|\boldsymbol{T}_r\|$. And in practice, usually two turbojet engines received command of the same rotor speed for convenience, which means $\|\boldsymbol{T}_r\| = \|\boldsymbol{T}_l\|$ and $T_{l3} - T_{r3} \approx 0$. Moreover, L_{T0} is small because most of the undesired rolling torques of two engines at the same rotor speed would be countered. As a result, $\|\boldsymbol{z}\|$ can be much smaller compared to $\|\boldsymbol{\tau}_u\|$. Therefore, $\boldsymbol{\tau}_u$ can be regarded as

the torque input for attitude control, and z can be regarded as a bounded disturbance. By using (1), we can rewrite the aircraft dynamics as:

$$\begin{cases} \dot{\boldsymbol{p}} = \boldsymbol{v}, \\ \dot{\boldsymbol{v}} = g\hat{\boldsymbol{e}}_3 - \dfrac{T_3}{m}\boldsymbol{R}(\boldsymbol{Q})^T\hat{\boldsymbol{e}}_3 - \dfrac{1}{ma_3}\boldsymbol{R}(\boldsymbol{Q})^T\boldsymbol{S}(\hat{\boldsymbol{e}}_3)\boldsymbol{\tau}_u, \end{cases} \tag{2}$$

$$\begin{cases} \dot{\boldsymbol{Q}} = \dfrac{1}{2}\begin{pmatrix} -\boldsymbol{q}^T \\ \eta\boldsymbol{I}_3 + \boldsymbol{S}(\boldsymbol{q}) \end{pmatrix}\boldsymbol{\omega}, \\ \boldsymbol{I}_f\dot{\boldsymbol{\omega}} = \boldsymbol{\tau}_u - \boldsymbol{S}(\boldsymbol{\omega})\boldsymbol{I}_f\boldsymbol{\omega} + z. \end{cases} \tag{3}$$

It can be seen that (2) is the position dynamics and (3) is the attitude dynamics. It should be noted that $\boldsymbol{\tau}_u$ is not only the control input of attitude dynamics, but also influences the position dynamics directly. This coupling between two dynamics leads to the non-minimum phase problem in VTOL control. To simplify the stability analysis, the following assumption is made:

Assumption 2: The mass m and torque lever arm a_3 are sufficiently large such that $ma_3 \gg 1$, so the coupling term $(ma_3)^{-1}R(\boldsymbol{Q})^T\boldsymbol{S}(\hat{\boldsymbol{e}}_3)\boldsymbol{\tau}_u \approx 0$.

Under *Assumption* 2, position dynamics (2) can be formulated as

$$\begin{cases} \dot{\boldsymbol{p}} = \boldsymbol{v}, \\ \dot{\boldsymbol{v}} = g\hat{\boldsymbol{e}}_3 - \dfrac{T_3}{m}\boldsymbol{R}(\boldsymbol{Q})^T\hat{\boldsymbol{e}}_3. \end{cases} \tag{4}$$

In this paper, the dynamics of engines and steers are ignored. It should be noted that torque input $\boldsymbol{\tau}_u$ only depends on T_1 and T_2, so the longitudinal thrust T_3 and $\boldsymbol{\tau}_u$ can be regarded as the independent control input of position dynamics (4) and attitude dynamics (3). According to the constrains $\|\boldsymbol{T}_r\| = \|\boldsymbol{T}_l\|$, $T_{l2} = T_{r2}$ and the definition of T_3 and $\boldsymbol{\tau}_u$, for any given $T_3 > 0$ and $\boldsymbol{\tau}_u$, $\boldsymbol{T}_r$ and $\boldsymbol{T}_l$ can be calculated through the following equations:

$$\begin{aligned} T_{r1} &= \left(0,\ -\frac{1}{2a_3}\ -\frac{1}{2a_2}\right)\boldsymbol{\tau}_u, \\ T_{l1} &= \left(0,\ -\frac{1}{2a_3},\ \frac{1}{2a_2}\right)\boldsymbol{\tau}_u, \\ T_{r2} = T_{l2} &= \left(\frac{1}{2a_3},\ 0,\ 0\right)\boldsymbol{\tau}_u, \\ T_{r3} &= \left(T_3^2 + T_{l1}^2 - T_{r1}^2\right)/2T_3, \\ T_{l3} &= \left(T_3^2 - T_{l1}^2 + T_{r1}^2\right)/2T_3. \end{aligned}$$

Therefore, in the rest of this paper, we use T_3 and $\boldsymbol{\tau}_u$ as the control input for discussion instead of $\boldsymbol{T}_r$ and $\boldsymbol{T}_l$.

Although fuel consumption of turbojet engines leads to changing mass and inertia tensor, the consumption rate would be much lower compared with the dynamics of our aircraft. Thus the following assumption is made about parameter uncertainty:

Assumption 3: The fuel is consumed at a relatively low rate so the mass m and inertia tensor $\boldsymbol{I}_f$ can be regarded as unknown constants in the aircraft dynamics.

Under *Assumption* 3, the mass m and the inertia tensor $\boldsymbol{I}_f$ can be estimated independently and regarded as constant parameters in the control design.

C. PROBLEM FORMATION

The objective of this paper is to design a globally asymptotic control law for the control input T_3 and $\boldsymbol{\tau}_u$, allowing the tailsitter aircraft to track a desired trajectory $\boldsymbol{p}_d(t)$. The tracking errors are defined as

$$\bar{\boldsymbol{p}}(t) \triangleq \boldsymbol{p}(t) - \boldsymbol{p}_d(t), \quad \bar{\boldsymbol{v}}(t) \triangleq \boldsymbol{v}(t) - \dot{\boldsymbol{p}}_d(t).$$

Our task is to design an estimation method for the unknown mass m independent of the control design first, thereby designing the control law guaranteeing the boundedness of T_3 and $\boldsymbol{\tau}_u$ in the presence of unknown inertia tensor $\boldsymbol{I}_f$ and bounded disturbance z. The following assumption is made about $\boldsymbol{p}_d(t)$, $\boldsymbol{I}_f$ and z:

Assumption 4: There exist positive constants λ_p, λ_I and λ_z such that $\left\|\boldsymbol{p}_d^{(n)}(t)\right\| \le \lambda_p$, $\|\boldsymbol{I}_f\| \le \lambda_I$ and $\|z(t)\| \le \lambda_z$ for all $t \ge 0$, where n is a positive integral satisfying $n \le 4$.

Similar to [24], the intermediary variable $\boldsymbol{F} \triangleq (\mu_1,\ \mu_2,\ \mu_3)^T$ and the error function $f(\boldsymbol{Q}, \boldsymbol{Q}_d)$ are used as the link between position and attitude dynamics, which are defined as:

$$\boldsymbol{F} \triangleq g\hat{\boldsymbol{e}}_3 - \frac{T_{3d}}{m}\boldsymbol{R}(\boldsymbol{Q}_d)^T\hat{\boldsymbol{e}}_3, \tag{5}$$

$$f(\boldsymbol{Q}, \boldsymbol{Q}_d) \triangleq \frac{T_3}{m}\boldsymbol{R}(\boldsymbol{Q})^T\hat{\boldsymbol{e}}_3 - \frac{T_{3d}}{m}\boldsymbol{R}(\boldsymbol{Q}_d)^T\hat{\boldsymbol{e}}_3, \tag{6}$$

where T_{3d} and $\boldsymbol{Q}_d \triangleq (\eta_d,\ \boldsymbol{q}_d^T)^T$ denote the desired longitudinal thrust and attitude quaternion. And then the position dynamics (4) can be rewritten as:

$$\begin{cases} \dot{\bar{\boldsymbol{p}}} = \bar{\boldsymbol{v}}, \\ \dot{\bar{\boldsymbol{v}}} = \boldsymbol{F} - \ddot{\boldsymbol{p}}_d - f(\boldsymbol{Q}, \boldsymbol{Q}_d). \end{cases} \tag{7}$$

Provided that the intermediary control input $\boldsymbol{F}$ is determined, T_{3d} and $\boldsymbol{Q}_d$ can be calculated through the following attitude extraction algorithm [25]:

$$\begin{aligned} T_{3d} &= m\left\|g\hat{\boldsymbol{e}}_3 - \boldsymbol{F}\right\|, \\ \eta_d &= \sqrt{\frac{1}{2} + \frac{m(g-\mu_3)}{2T_{3d}}}, \quad \boldsymbol{q}_d = \frac{m}{2T_{3d}\eta_d}\begin{pmatrix} \mu_2 \\ -\mu_1 \\ 0 \end{pmatrix}, \end{aligned} \tag{8}$$

under the condition that

$$\boldsymbol{F} \ne (0,\ 0,\ x)^T, \quad \text{for } x \ge g. \tag{9}$$

Condition (9) indicates that the engines should not be shut down or generate thrust in the same direction as gravity, which is reasonable in practice. Through (8) it is easy to see that the boundedness of $\boldsymbol{F}$ indicates the boundedness of T_3, and if $\boldsymbol{F}$ is differentiable, the desired angular velocity of the aircraft can be formulated as:

$$\boldsymbol{\omega}_d = \boldsymbol{\Xi}(\boldsymbol{F})\dot{\boldsymbol{F}}, \tag{10}$$

$$\dot{\boldsymbol{\omega}}_d = \dot{\boldsymbol{\Xi}}(\boldsymbol{F})\dot{\boldsymbol{F}} + \boldsymbol{\Xi}(\boldsymbol{F})\ddot{\boldsymbol{F}}, \tag{11}$$

where $\Xi(F)$ and $\dot{\Xi}(F)$ are matrixes depending on F and $\dot{F}$ respectively, and related details are given in APPENDIX. Provided that $F, \dot{F}$ and $\ddot{F}$ are all bounded, then $\Xi(F)$ and $\dot{\Xi}(F)$ are bounded. From (10), (11) it can be concluded that ω_d and $\dot{\omega}_d$ are bounded as well.

Provided that the desired attitude Q_d and ω_d are determined, the attitude tracking error $\bar{Q} \triangleq (\bar{\eta}, \bar{q}^T)^T$ is defined as

$$\bar{Q} = Q_d^{-1} \odot Q, \tag{12}$$

and the attitude error dynamics is defined as

$$\begin{cases} \dot{\bar{Q}} = \frac{1}{2} \begin{pmatrix} -\bar{q}^T \\ \bar{\eta} I_3 + S(\bar{q}) \end{pmatrix} \bar{\omega}, \\ \bar{\omega} = \omega - R(\bar{Q}) \omega_d, \\ I_f \dot{\omega} = \tau_u - S(\omega) I_f \omega + z. \end{cases} \tag{13}$$

Since the dynamics of engines are not taken into consideration in this paper, the longitudinal thrust T_3 is supposed to equal to T_{3d} immediately, and then (6) can be rewritten as:

$$\begin{aligned} f(Q, Q_d) &= \frac{T_{3d}}{m} R(Q)^T \left(I_3 - R(\bar{Q}) \right) \hat{e}_3 \\ &= \frac{2T_{3d}}{m} R(Q)^T S(\hat{q}) \bar{q}, \end{aligned} \tag{14}$$

where $\hat{q} = (\bar{q}_2, -\bar{q}_1, -\bar{\eta})^T$. From (14) and the boundedness of T_3 it is easy to see that $\bar{Q} \to (\pm 1, 0, 0, 0)^T$ indicates $f(Q, Q_d) \to 0$.

III. CONTROL DESIGN

A. MASS ESTIMATION BASED ON COMPLEMENTARY FILTER

Although the mass of our aircraft is unknown, there are serveral useful methods to estimate it in application. It should be noted that the fuel consumption of turbojet engines is the main reason for mass change, so the following equation can be established:

$$\dot{m} = -f_c,$$

where f_c denotes the rate of fuel consumption. Through the analysis of ground experiment data in [29], we can find that there is a linear relationship between the rate of fule consumption f_c and the rotor speed n_T when the thrust changes in a small scope, modeled by the following equation:

$$f_c(n_T) = \beta_T n_T + \beta_0,$$

where β_T and β_0 are constant parameters, and n_T can be measured accurately by the hall sensor. Let $\hat{f}_c$ denote the estimated rate of fuel consumption, which can be formulated by the following equation:

$$\hat{f}_c(n_T) = \hat{\beta}_T n_T + \hat{\beta}_0,$$

where $\hat{\beta}_T$ and $\hat{\beta}_0$ are constant parameters modeled from the ground experiment. In the presence of modeling error, it is usual to obtain $\hat{\beta}_T \neq \beta_T$ and $\hat{\beta}_0 \neq \beta_0$. Then the modeling error e_f can be formulated by the following equation:

$$e_f \triangleq f_c(n_T) - \hat{f}_c(n_T) = (\beta_T - \hat{\beta}_T) n_T + \beta_0 - \hat{\beta}_0.$$

By integrating $\hat{f}_c$, we can obtain the estimate of the UAV's mass, denoted by $\bar{m}_b$. However, the modeling error e_f is also integrated, leading to the estimate diverging over time.

Another method for mass estimation relies on Newton second law of motion. Let $\bar{m}$ and a_m denoted the estimated mass and the acceleration measured by the accelerometer respectively. Assuming the thrust of turbojet engines is the only force imposed on our UAV except the gravity force, the estimate of mass can be calculated by the following equation:

$$\bar{m} = \frac{\|T\|}{\|a_m\|},$$

where T is the thrust vector. It should be noted that in the presence of vibration and other external disturbances, some high-frequency noises are added to this estimated value.

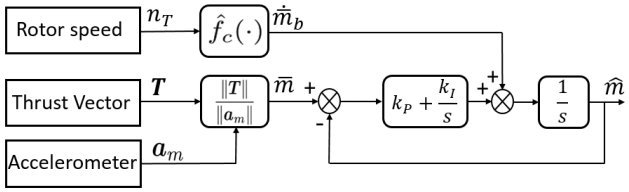

FIGURE 5. Explicit complementary filter.

In order to get a better estimation result, a complementary filter is designed to combine the two estimate value $\bar{m}_b$ and $\bar{m}$ to obtain a new estimate value $\hat{m}$. This complementary filter is based on the attitude estimation approach in flight control [30]. The main idea is to design a high-pass filter on $\bar{m}_b$ and a low-pass filter on $\bar{m}$. The block diagram of this complementary filter is shown in Fig. 5. A classical proportional integral compensation is adopted in this filter. The parameter k_P is used to adjust the cross frequency of high-pass and low-pass filtering, while the parameter k_I is used to compensate the integral error of $\bar{m}_b$. The mathematical relation of $\hat{m}$, $\dot{\bar{m}}_b$ and $\bar{m}$ in Lapalace form (with Laplace operator s) are as follows:

$$\hat{m} = \frac{1}{s} \dot{\bar{m}}_b + \frac{k_p}{s} \left(\bar{m} - \hat{m} \right) + \frac{k_I}{s^2} \left(\bar{m} - \hat{m} \right). \tag{15}$$

The error equation of $\hat{m}$ can be formulated as:

$$\delta \hat{m} = \frac{s \delta \dot{\bar{m}}_b + \left(k_p s + k_i \right) \delta \bar{m}}{s^2 + k_p s + k_i}. \tag{16}$$

According to equation (16) and the final value theorem, it is easy to see that the estimated mass error converges to the error of the mass calculated from the accelerometer:

$$\lim_{t \to \infty} \delta \hat{m} = \delta \bar{m}, \tag{17}$$

which indicates that in a short time the filter uses the estimated rate of fuel consumption to improve estimation accuracy of mass, while in a long time the estimated mass

error is limited within a certain range by using the data from accelerometer. This complementary filter is able to overcome the adverse effect caused by high-frequency noises and the integral error. Since the estimation of mass is independent to the control law, it is reasonable to consider m as a known parameter in the following control design.

B. INTERMEDIARY POSITION CONTROL DESIGN

First we introduce the non-decreasing differentiable scalar saturation function $\sigma_i(x)$ for scalar $x \in \mathbb{R}$, which is defined as:

$$\begin{aligned}
&\text{(a)}\ x\sigma_i(x) \geq 0, \quad \forall x \\
&\text{(b)}\ \sigma_i(x) = k_i x, \quad \forall |x| \leq l_i \\
&\text{(c)}\ \sigma_i(x) = M_i\,(\text{sign}(x)), \quad \forall |x| \geq L_i \\
&\text{(d)}\ 0 \leq \frac{\partial \sigma_i(x)}{\partial x} \leq k_i, \quad \forall x \\
&\text{(e)}\ \left|\frac{\partial^2 \sigma_i(x)}{\partial^2 x}\right| \leq \frac{M_i - k_i l_i}{L_i - l_i}, \quad \forall x
\end{aligned} \tag{18}$$

where k_i, l_i, M_i and L_i are some positive design parameters with $M_i > k_i l_i$ and $L_i > l_i$. For any given vector $\hat{\boldsymbol{x}} \triangleq (x_1,\ x_2,\ x_3)^T$, the vector saturation function $\hat{\boldsymbol{\sigma}}_i(\hat{\boldsymbol{x}})$ is defined as:

$$\hat{\boldsymbol{\sigma}}_i(\hat{\boldsymbol{x}}) = \begin{pmatrix} \sigma_i(x_1) \\ \sigma_i(x_2) \\ \sigma_i(x_3) \end{pmatrix}, \tag{19}$$

where $\sigma_i(\cdot)$ is the saturation function defined in (18).

Motivated by [16], the intermediary control input $\boldsymbol{F}$ is designed as:

$$\boldsymbol{F} = \ddot{\boldsymbol{p}}_d - \hat{\boldsymbol{\sigma}}_2(\bar{\boldsymbol{v}} + \hat{\boldsymbol{\sigma}}_1(\bar{\boldsymbol{p}})), \tag{20}$$

where $\hat{\boldsymbol{\sigma}}_1(\cdot)$ and $\hat{\boldsymbol{\sigma}}_2(\cdot)$ represent the vector saturation function defined in (19) satisfying the following conditions:

$$\begin{aligned}
&k_1 l_1 > l_2, \\
&k_2 l_2 > \frac{T_m}{m}\gamma_T + k_1(l_2 + M_1),
\end{aligned} \tag{21}$$

where T_m denotes the upper bound of T_3, and γ_T is a positive constant satisfying $\gamma_T < 1$. It is easy to see that $\boldsymbol{F}$, $\dot{\boldsymbol{F}}$, $\ddot{\boldsymbol{F}}$ are all bounded, and according to (8), (10) and (11), the desired variables T_{3d}, $\boldsymbol{\omega}_d$ and $\dot{\boldsymbol{\omega}}_d$ are bounded as well. The following assumption is made:

Assumption 5: $T_m \geq m(g + \lambda_p + M_2)$.

Loosely speaking, *Assumption* 5 states that the available thrust is large enough such that the desired intermediary control law (20) is feasible. And to satisfy (21) the following condition holds:

$$\gamma_T < \frac{k_2 l_2 - k_1(l_2 + M_1)}{g + \lambda_p + M_2}. \tag{22}$$

Under *Assumption* 5, there always exist a set of parameters satisfying (21) and (22) simultaneously.

C. ATTITUDE CONTROL DESIGN

According to the boundedness of $\boldsymbol{\omega}_d$ and $\dot{\boldsymbol{\omega}}_d$, there exist positive constants $\lambda_{\omega 1}$ and $\lambda_{\omega 2}$ satisfying $\|\boldsymbol{\omega}_d(t)\| \leq \lambda_{\omega 1}$ and $\|\dot{\boldsymbol{\omega}}_d(t)\| \leq \lambda_{\omega 2}$ for all $t \geq 0$. Similar to [21], for attitude dynamics (13) the control input torque $\boldsymbol{\tau}_u \triangleq (u_1,\ u_2,\ u_3)^T$ is designed as:

$$\begin{cases} u_i = -\dfrac{u_m s_i}{|s_i| + k^2\delta}, \quad i = 1,\ 2,\ 3 \\ \boldsymbol{s} \triangleq (s_1,\ s_2,\ s_3)^T = \bar{\boldsymbol{\omega}} + k^2 \bar{\boldsymbol{q}}, \end{cases} \tag{23}$$

where u_m and δ are positive constants, and k is an adaptive variable to ensure asymptotic disturbance rejection. The error quaternion vector $\bar{\boldsymbol{q}} \triangleq (\bar{q}_1,\ \bar{q}_2,\ \bar{q}_3)^T$ and the error angular velocity $\bar{\boldsymbol{\omega}} \triangleq (\bar{\omega}_1,\ \bar{\omega}_2,\ \bar{\omega}_3)^T$ are calculated through (12) and (13) respectively. The adaptive law of $k(t)$ is designed as:

$$\begin{aligned}
\dot{k} = \frac{\gamma k}{1 + 4\gamma(1 - \bar{\eta})}\Bigg\{ u_m \sum_{i=1}^{3}\Bigg[&\frac{\bar{\omega}_i \bar{q}_i}{|s_i| + k^2\delta} \\
&- \frac{|\bar{\omega}_i|\,(1+\delta)}{|\bar{\omega}_i| + k^2(1+\delta)}\Bigg] - \boldsymbol{q}^T \boldsymbol{s}\Bigg\}.
\end{aligned} \tag{24}$$

The parameter γ is a sufficiently small positive constant satisfying the following condition:

$$\gamma\Big[\big(u_m(1+\delta)/\delta + c_k(\gamma)^2\big)c_1(\gamma) + c_2(\gamma)\Big] \leq (k_0^2 - \bar{k}^2), \tag{25}$$

where k_0 denotes the initial value of $k(t)$ and $\bar{k}$ is a positive constant satisfying $\bar{k} < k_0$. $c_k(\gamma)$, $c_1(\gamma)$ and $c_2(\gamma)$ are positive functions satisfying

$$\begin{aligned}
k(t) < c_k(\gamma), \quad \forall t, \quad &\int_0^\infty \|\bar{\boldsymbol{\omega}}(x)\|\,\mathrm{d}x < c_1(\gamma), \\
&\int_0^\infty k^4(x)\bar{\boldsymbol{q}}^T(x)\bar{\boldsymbol{q}}(t)\mathrm{d}x < c_2(\gamma).
\end{aligned} \tag{26}$$

It is clear that the control input $\boldsymbol{\tau}_u$ is bounded by $\pm u_m$. The following assumption is made:

Assumption 6: $u_m > \lambda_I(\lambda_{\omega 1}^2 + \lambda_{\omega 2}) + \lambda_z$.

In fact, *assumption* 6 states that the available control torque is sufficient to simultaneously track the desired attitude $\boldsymbol{Q}_d$ and angular velocity $\boldsymbol{\omega}_d$ with rejecting bounded disturbances.

IV. STABILITY ANALYSIS

In this section, the global asymptotic stability of the tracking error system is proven. We demonstrate in Theorem 1 that the states of position dynamics (7) with the intermediary control law (20) are ultimately bounded by the error function $f(\boldsymbol{Q}, \boldsymbol{Q}_d)$ under some conditions. And then in Theorem 2 it is proved that the attitude dynamics (13) with the control law (23) and the adaptive law (24) is globally asymptotically stable. The stability of the whole system is a direct conclusion of these two theorems.

For any scalar value $\tilde{x}(t) \in R$ and $\lambda \in R^+$, we write $\tilde{x}(t) \approx O(\lambda)$ to denote that $\tilde{x}(t)$ and λ have the same order. Before proving the ultimate boundedness of position error dynamics,

we first demonstrate the ultimate boundedness of a simple scalar system in the following lemma:

Lemma 1: Consider the following system

$$\begin{cases} \dot{\tilde{x}}_1 = \tilde{x}_2, \\ \dot{\tilde{x}}_2 = u + d(t). \end{cases} \tag{27}$$

with states $(\tilde{x}_1, \tilde{x}_2) \in \mathbb{R} \times \mathbb{R}$, *disturbance* $d(t)$: $\mathbb{R}^+ \to \mathbb{R}$, *and control law*

$$u \triangleq -\sigma_2(\tilde{x}_2 + \sigma_1(\tilde{x}_1)), \tag{28}$$

where σ_1 *and* σ_2 *are the saturation functions defined in* (18). *If the parameters satisfy the following conditions*:

$$\begin{aligned} &k_1 l_1 > l_2, \\ &k_2 l_2 > \lambda_d + k_1(l_2 + M_1), \end{aligned} \tag{29}$$

where λ_d *denotes the upper bound of* $|d(t)|$, *then the states* $(\tilde{x}_1, \tilde{x}_2)$ *are ultimately bounded by* $O(\lambda_d)$.

Proof: It is easy to see that if all states reach the linear unsaturated region of the saturation function in a finite time, then the system (27) becomes

$$\begin{aligned} \begin{bmatrix} \dot{\tilde{x}}_1 \\ \dot{\tilde{x}}_2 \end{bmatrix} &= \boldsymbol{A} \begin{bmatrix} \tilde{x}_1 \\ \tilde{x}_2 \end{bmatrix} + \begin{bmatrix} 0 \\ d(t) \end{bmatrix}, \\ \boldsymbol{A} &= \begin{bmatrix} 0 & 1 \\ -k_1 k_2 & -k_2 \end{bmatrix}. \end{aligned} \tag{30}$$

Since $\boldsymbol{A}$ is a Hurwitz matrix, for initial time t_u there always exist positive constants a and b satisfying

$$\|\tilde{x}(t)\| \leq a e^{-b(t-t_0)} \|\tilde{x}(t_0)\| + \frac{a}{b}\lambda_d \,,$$

which indicates the Input-to-State stability on $d(t)$, so to complete the proof we only need to demonstrate that all states reach the linear unsaturated region in a finite time.

Let $y = \tilde{x}_2 + \sigma_1(\tilde{x}_1)$, first we show that $y(t)$ reach the region $\Omega_2 \triangleq \{y : |y| \leq l_2\}$ in a finite time. For initial time t_0, assum $y(t_0) \geq l_2$ without loss of generality. If $y(t)$ does not reach Ω_2 in a finite time, using (28) and (29), we obtain

$$\begin{aligned} \dot{\tilde{x}}_2 &= -\sigma_2(y) + d(t) \\ &\Rightarrow \dot{\tilde{x}}_2 \leq -k_2 l_2 + d(t) \\ &\Rightarrow \tilde{x}_2(t) \leq \tilde{x}_2(t_0) - (k_2 l_2 - \lambda_d)t \\ &\Rightarrow y(t) \leq y(t_0) + \sigma_1\left(\tilde{x}_1(t)\right) \\ &\quad - \sigma_1\left(\tilde{x}_1(t_0)\right) - (k_2 l_2 - \lambda_d)t \\ &\Rightarrow y(t) \leq y(t_0) + 2M_1 - (k_2 l_2 - \lambda_d)t. \end{aligned} \tag{31}$$

The right-hand side of the last equation in (31) goes to negative infinity as $t \to \infty$, leading to a contradiction with the assumption. Thus $y(t)$ reaches Ω_2 in a finite time, and we can obtain the upper-bound of this reaching time t_1:

$$t_1 \leq t_0 + \frac{y(t_0) + 2M_1 - l_2}{k_2 l_2 - \lambda_d}.$$

Then we show $y(t)\dot{y}(t) < 0$ at the boundaries of Ω_2. Under the condition $|y(t)| = l_2$, using (28) and (29) we obtain

$$\begin{aligned} y\dot{y} &= y\left(-\sigma_2(y) + d(t) + \frac{\partial \sigma_1(\tilde{x}_1)}{\partial x_1}\dot{\tilde{x}}_1\right) \\ &= y\left(-k_2 l_2 \mathrm{sign}(y) + d(t) + \frac{\partial \sigma_1(\tilde{x}_1)}{\partial x_1}\left(y - \sigma_1(\tilde{x}_1)\right)\right) \\ &\leq |y|\left(-k_2 l_2 + \lambda_d + k_1(l_2 + M_1)\right) < 0. \end{aligned}$$

This proves Ω_2 is positively invariant.

Next, the same technique is used to prove that $\tilde{x}_1(t)$ would reach the region $\Omega_1 \triangleq \{y : |y| \leq l_1\}$ in a finite time. Without loss of generality, assum $\tilde{x}_1(t_1) \geq l_1$. If $\tilde{x}_1(t)$ does not reach Ω_1 in a finite time, using (28) we obtain

$$\begin{aligned} \dot{\tilde{x}}_1(t) &= y(t) - \sigma_1\left(\tilde{x}_1(t)\right) \\ &\leq l_2 - k_1 l_1 \\ &\Rightarrow \tilde{x}_1(t) \leq \tilde{x}_1(t_1) - (k_1 l_1 - l_2)(t - t_1). \end{aligned} \tag{32}$$

where the right-hand side of the last equation goes to negative infinity as $t \to \infty$, so $\tilde{x}_1(t)$ reaches Ω_1 in a finite time, and we can obtain the upper-bound of the time point t_2:

$$t_2 \leq t_1 + \frac{\tilde{x}_1(t_1) - l_1}{k_1 l_1 - l_2}.$$

And under the condition $|\tilde{x}_1(t)| = l_1$, we have

$$\begin{aligned} \tilde{x}_1\dot{\tilde{x}}_1 &= \tilde{x}_1\left(y - \sigma_1\left(\tilde{x}_1\right)\right) \\ &= \tilde{x}_1\left(y - k_1 l_1 \mathrm{sign}(\tilde{x}_1)\right) \\ &\leq |\tilde{x}_1|\left(l_2 - k_1 l_1\right) < 0. \end{aligned}$$

This indicates that Ω_1 is positively invariant and completes the proof. ■

Lemma 1 simplifies the proof for the following theorem:

Theorem 1: Consider the closed-loop error system (7) *with the intermediary control law* (20) *satisfying the condition* (21). *If there exist some* $\epsilon > 0$ *and* $t_f > 0$ *such that* $\left\|f(\boldsymbol{Q}, \boldsymbol{Q}_d)\right\| \leq \epsilon$ *for all* $\boldsymbol{Q}(t)$, $\boldsymbol{Q}_d(t)$ *with* $t > t_f$, *and the following condition holds*:

$$\epsilon < \frac{T_m}{m}\gamma_T, \tag{33}$$

then the states $(\bar{\boldsymbol{p}}, \bar{\boldsymbol{v}}) \in \mathbb{R}^3 \times \mathbb{R}^3$ *of system* (7) *are ultimately bounded by* $O(\epsilon)$.

Proof: It should be noted that the system (27) with the control law (28) is just the scalar form of the position error dynamics (7) with the control law (20). For $t > t_f$, $f(\boldsymbol{Q}, \boldsymbol{Q}_d)$ can be regarded as the disturbance bounded by $\lambda_d \triangleq \epsilon$, and from (21) and (33) the conditions (29) hold. According to Lemma 1, the states $(\bar{\boldsymbol{p}}, \bar{\boldsymbol{v}})$ are ultimately bounded by $O(\epsilon)$. ■

Theorem 1 states that if $f(\boldsymbol{Q}, \boldsymbol{Q}_d)$ is bounded by a sufficiently small positive constant ϵ after a finite time, the tracking error is ultimately bounded. Moreover, if $\lim_{t\to\infty} f(\boldsymbol{Q}, \boldsymbol{Q}_d) = 0$, the tracking error is also approximating zero and the whole system is asymptotically stable. To illustrate this, the following theorem is presented:

Theorem 2: Consider the attitude error system (13) *with the control law* (23) *and adaptive law* (24). *If a sufficiently small* γ *satisfying condition* (25) *is chosen, then* $\lim_{t\to\infty}\bar{\boldsymbol{\omega}}(t) = \lim_{t\to\infty}\bar{\boldsymbol{q}} = 0$, *and moreover,* $\lim_{t\to\infty} f(\boldsymbol{Q}, \boldsymbol{Q}_d) = 0$.

Proof: Similar to [21], the following Lyapunov function is chosen:

$$V = \frac{1}{2}\left(\bar{\boldsymbol{\omega}}^T \boldsymbol{I}_f \bar{\boldsymbol{\omega}} + 2k^2\left(\bar{\boldsymbol{q}}^T\bar{\boldsymbol{q}} + (\bar{\eta}-1)^2\right) + k^2/\gamma\right). \quad (34)$$

Using (23) and (24), we can obtain

$$\dot{V} \le -\|\bar{\boldsymbol{\omega}}\|\left(u_m - \|\boldsymbol{H}\| - \lambda_z\right) - k^4\bar{\boldsymbol{q}}^T\bar{\boldsymbol{q}}, \quad (35)$$

where $\boldsymbol{H} \triangleq (\boldsymbol{R}(\bar{\boldsymbol{Q}})\boldsymbol{\omega}_d)\times\boldsymbol{I}_f(\boldsymbol{R}(\bar{\boldsymbol{Q}})\boldsymbol{\omega}_d) + \boldsymbol{I}_f(\boldsymbol{R}(\bar{\boldsymbol{Q}})\dot{\boldsymbol{\omega}}_d)$. It should be noted that pre-multiplying any vector by the rotation matrix $\boldsymbol{R}(\bar{\boldsymbol{Q}})$ will lead to a new vector with the same magnitude of the old one, which means $\left\|\boldsymbol{R}(\bar{\boldsymbol{Q}})\boldsymbol{\omega}_d\right\| = \|\boldsymbol{\omega}_d\| \le \lambda_{\omega 1}$ and $\left\|\boldsymbol{R}(\bar{\boldsymbol{Q}})\dot{\boldsymbol{\omega}}_d\right\| = \|\dot{\boldsymbol{\omega}}_d\| \le \lambda_{\omega 2}$. According to *Assumption* 4, we can obtain $\left\|\boldsymbol{I}_f\right\| \le \lambda_I$. So the following relation holds:

$$\begin{aligned}\|\boldsymbol{H}\| &\le \left\|\boldsymbol{R}(\bar{\boldsymbol{Q}})\boldsymbol{\omega}_d\right\|\left\|\boldsymbol{I}_f\right\|\left\|\boldsymbol{R}(\bar{\boldsymbol{Q}})\boldsymbol{\omega}_d\right\| \\ &\quad + \left\|\boldsymbol{I}_f\right\|\left\|\boldsymbol{R}(\bar{\boldsymbol{Q}})\dot{\boldsymbol{\omega}}_d\right\| \quad (36)\\ &= \|\boldsymbol{\omega}_d\|\left\|\boldsymbol{I}_f\right\|\|\boldsymbol{\omega}_d\| + \left\|\boldsymbol{I}_f\right\|\|\dot{\boldsymbol{\omega}}_d\| \\ &\le \left(\lambda_{\omega 1}^2 + \lambda_{\omega 2}\right)\lambda_I. \quad (37)\end{aligned}$$

Under *Assumption* 6, applying the relation (37) to the inequality (35) we finally obtain $\dot{V} \le 0$, which implies that $\bar{\boldsymbol{\omega}}$ and k are all bounded. As a result, V is bounded. Define $c \triangleq u_m - \lambda_I(\lambda_{\omega 1}^2 + \lambda_{\omega 2}) - \lambda_z$. By integrating (35) we obtain

$$V(0) - V(\infty) \ge c\int_0^\infty \|\bar{\boldsymbol{\omega}}(x)\|\,\mathrm{d}x + \int_0^\infty k^4(x)\bar{\boldsymbol{q}}^T(x)\bar{\boldsymbol{q}}(x)\mathrm{d}x. \quad (38)$$

Because the term on the left-hand side is bounded, it follows that $\bar{\boldsymbol{\omega}} \in \mathcal{L}^1$ and $k^2\eta \in \mathcal{L}^2$. From the boundedness of $\bar{\boldsymbol{\omega}}$, k and $\bar{\boldsymbol{q}}$, it is easy to see that $\dot{k}$, $\dot{\bar{\boldsymbol{\omega}}}$ and $\dot{\bar{\boldsymbol{q}}}$ are all bounded, as well as $c_k(\gamma)$, $c_1(\gamma)$ and $c_2(\gamma)$ are finite functions. Using the Barbalat's lemma we obtain

$$\lim_{t\to\infty}\bar{\boldsymbol{\omega}}(t) = \lim_{t\to\infty} k^2(t)\bar{\boldsymbol{q}} = \lim_{t\to\infty}\boldsymbol{s} = 0, \quad (39)$$

which indicates that there exist constants g_1 and g_2 such that $\|\bar{\boldsymbol{\omega}}(t)\| \le g_1$ and $\|\boldsymbol{s}\| \le g_2$ hold for all $t \ge 0$. From(24), with the same derivation in [21] we obtain

$$\dot{k} \ge -\gamma k\left[3u_m\left(1+\frac{1}{\delta}\right)(2+\delta) + g_2\right].$$

This inequality can be integrated to obtain

$$k(t) \ge k_0\exp(-\gamma\xi t), \quad (40)$$

where $\xi \triangleq 3u_m\left(1+\frac{1}{\delta}\right)(2+\delta) + g_2$. This indicates $k(t) \ge 0$ for all time with $k(t) = 0$ possible only at $t = \infty$.

From (24) we can also obtain the following inequality:

$$k\dot{k} \ge -\gamma\left[\left(u_m\frac{1+\delta}{\delta} + c_k(\gamma)^2\right)\|\bar{\boldsymbol{\omega}}\| + k^4\bar{\boldsymbol{q}}^T\bar{\boldsymbol{q}}\right].$$

TABLE 1. Controller parameters.

k_1	k_2	l_1	l_2	L_1	L_2	M_1	M_2
0.66	0.86	10	65	20	70	12	60

γ_T	γ	δ	u_m	k_p	k_I
0.02	0.01	0.5	20	1	0.15

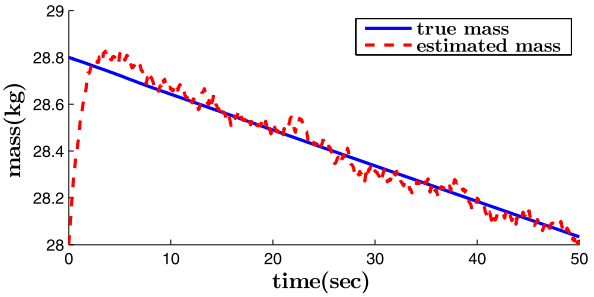

FIGURE 6. The true mass and the estimated mass through complementary filter vs. time.

By integrating this inequality we obtain

$$k^2(\infty) \ge k_0^2 - 2\gamma\left[\left(u_m\frac{1+\delta}{\delta} + c_k(\gamma)^2\right)\int_0^\infty\|\bar{\boldsymbol{\omega}}(x)\|\,\mathrm{d}x + \int_0^\infty k^4(x)\bar{\boldsymbol{q}}^T(x)\bar{\boldsymbol{q}}(x)\mathrm{d}x\right].$$

Hence if a sufficiently small positive constantγ satisfying the condtion (25) is found, then $k(t) \ge \bar{k}$ hold for all $t \ge 0$. Therefore, $\lim_{t\to\infty} k^2(t)\bar{\boldsymbol{q}} = 0$ leads to $\lim_{t\to\infty}\bar{\boldsymbol{q}} = 0$. According to (14), we obtain $\lim_{t\to\infty} f(\boldsymbol{Q}, \boldsymbol{Q}_d) = 0$, which completes the proof. ■

From Theorem 1 and Theorem 2, it is concluded that the tracking error system (7), (13) with the intermediary controller (20) and the adaptive attitude controller (23), (24) satisfying conditions (21), (25) is globally asymptotically stable.

V. SIMULATION RESULTS

We use SIMULINK as the simulation tool to illustrate the effectiveness of the proposed control scheme. As described in Section III-A, the changing rate of the mass is considered as a linear function of the thrust, and the modeling error is set as $\hat{\beta}_T - \beta_T = 4.75\times10^{-5}$ and $\hat{\beta}_0 - \beta_0 = 0.002$. White Gaussian noises are added to the measured acceleration with variance 0.0005. The initial values of mass and estimated mass are 28.8 kg and 28 kg respectively. All initial states of the aircraft are set to zero except the initial attitude quaternion, which is set to $(0.9,\ 0.2517,\ 0.2517,\ -0.2517)^T$. The initial adaptive parameter $k(0)$ is set to 1. The inertia tensor is set to $\left((20,\ 2,\ 0.9)^T,\ (2,\ 17,\ 0.5)^T,\ (0.9,\ 0.5,\ 15)^T\right)$, which remains unchanged according to *Assumption* 3. The moment disturbance z caused by the two different longitudinal thrusts is considered as a gaussian noise, the variance of which is proportional to thrust with the scaling factor $p_T = 0.0005$ m. The desired trajectory is set as $\boldsymbol{p}_d(t) = (20\cos(0.2t+2),\ 20\sin(0.2t+2.4),\ 4t)^T$ m. Let $T_m = 400$ N and $u_m = 20\,\mathrm{N}\cdot m$ denote the maximum

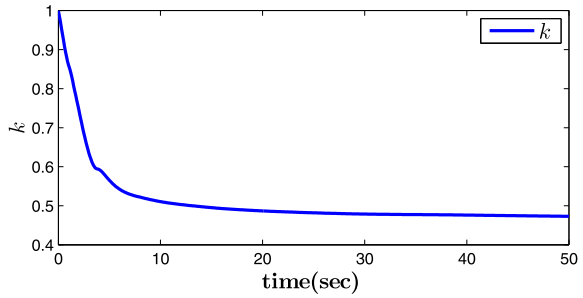

FIGURE 7. The adaptive parameter k vs. time.

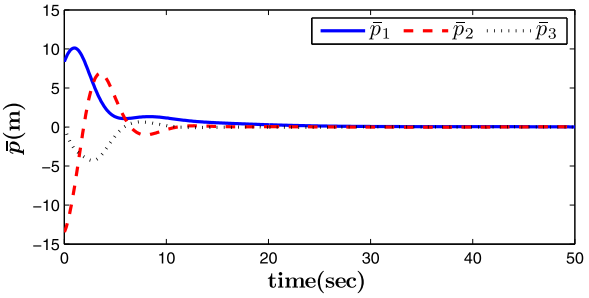

FIGURE 8. Position tracking error vs. time.

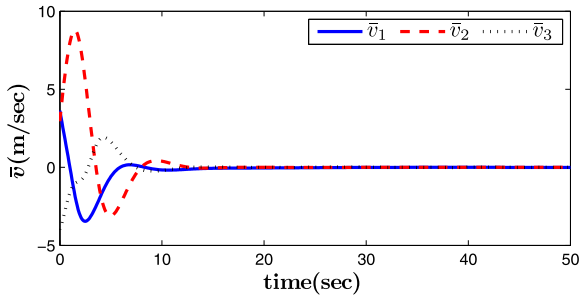

FIGURE 9. Velocity tracking error vs. time.

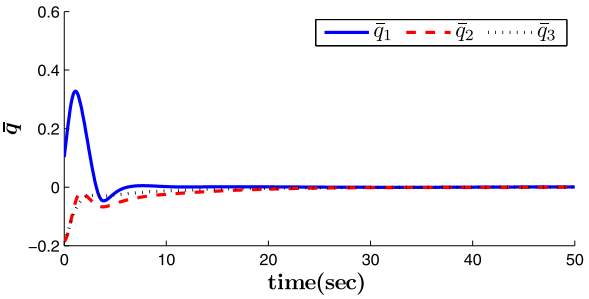

FIGURE 10. Attitude tracking error vs. time.

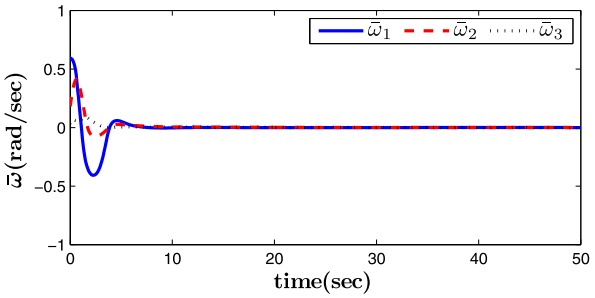

FIGURE 11. Angular velocity tracking error vs. time.

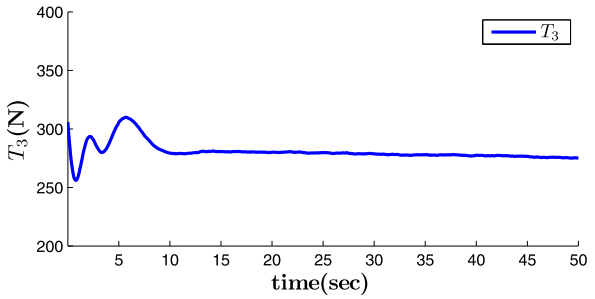

FIGURE 12. Thrust vs. time.

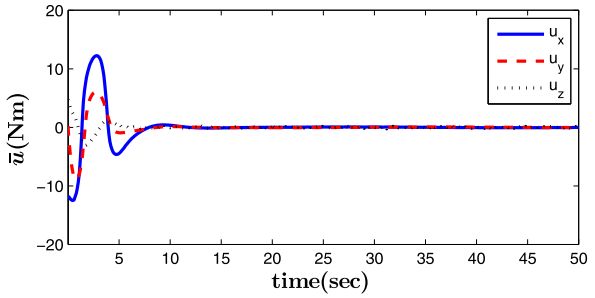

FIGURE 13. Control torque vs. time.

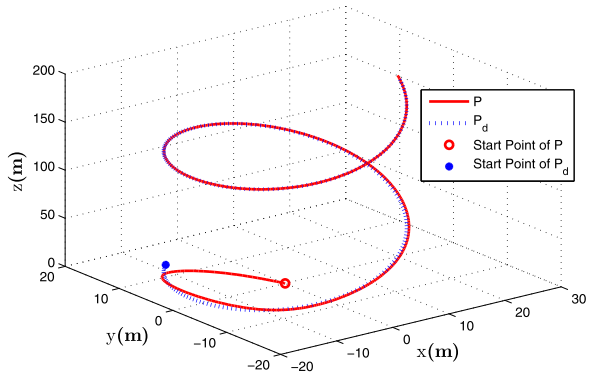

FIGURE 14. 3D plot of the VTOL vehicle trajectory (red) with the desired trajectory (blue).

of thrust and control torque. The controller parameters are chosen as shown in Table 1 to satisfy the conditions (9), (21), (22) and (25) and (29). The simulation results are presented in Figs. 6∼14.

Fig. 6 shows that the estimated mass converges rapidly to the true value and the estimated mass error converges to the error of the mass calculated according to accelerometer data. By adjusting the PI parameters we are able to adjust the convergence speed. From Fig. 7 it is clear that the adaptive paramter $k(t)$ asymptotically converges to a positive value. Figs. 8, 9, 10 and 11 illustrate that the position tracking error, velocity tracking error, attitude tracking error and angular velocity tracking error asymptotically converge to zero respectively. From Fig. 12 and Fig. 13, it can be seen that the

FIGURE 15. The tailsitter aircraft in the experiment.

control input thrust and torque are limited by the saturation function, which satisfies $T_3 \leq T_m$, $|u_1| \leq u_m$, $|u_2| \leq u_m$, $|u_3| \leq u_m$. In Fig. 14, a 3-D plot of the UAV's position with the desired trajectory is given to illustrate the position tracking. From these figures, it is clear that the asymptotic stability is guaranteed in the presence of input boundedness and parameter uncertainty.

VI. CONCLUSION

In this paper, we first introduce the tailsitter VTOL UAV equipped with the thrust-vectoring propulsion system and then design an adaptive control approach by combining the nested saturation function and variable structure techniques for this UAV to solve the input boundedness problem. An explicit complementary filter is utilized to solve the mass uncertainty problem. The disturbances on control torque are rejected through the adaptive attitude control approach. Some assumptions are made to simplify the model, and under these assumptions the global asymptotic stability of the closed-loop system is proven. Simulation results are presented to illustrate the effectiveness of our method. With simple modification, this control method can be applied to other tailsitter models equipped with different thrust-vectoring propulsion systems.

Future work will concentrate on pratical experiments. As shown in Fig. 15, we have assembled a real tailsitter VTOL UAV equipped with the thrust-vectoring propulsion system described in Section II-A. During the experiments, it was found that the disturbances caused by wind have become the main problem for our position tracking control. Sometimes the wind is so strong that our adaptive controller becomes invalid in the presence of input boundedness. Right now, we are trying to find some new control strategies based on the adaptive controller presented in this paper to reduce the disturbances from wind. For example, by adjusting the attitude of our aircraft, especially the roll angle, we could dramtically reduce the disturbances caused by the wind in a certain direction. Besides, we ignore the dynamics of our thrust-vectoring propulsion system in this paper. However, there is a time lag between command sending and engine response, which limits the changing rate of the thrust. In the future, a more comprehensive model will be built by taking the dynamics of our thrust-vectoring propulsion system into account, which allows us to design a more practical controller for experiments.

APPENDIX

We derive the boundedness of angular velocity $\boldsymbol{\omega}_d$ and angular acceleration $\dot{\boldsymbol{\omega}}_d$ from (10) and (11) in this part. According to [25], the function $\boldsymbol{\Xi}(\boldsymbol{F})$ is in the following form:

$$\boldsymbol{\Xi}(\boldsymbol{F}) = \frac{1}{\gamma_1^2\gamma_2}\begin{pmatrix} -\mu_1\mu_2 & -\mu_2^2+\gamma_1\gamma_2 & \mu_2\gamma_2 \\ \mu_1^2-\gamma_1\gamma_2 & \mu_1\mu_2 & -\mu_1\gamma_2 \\ \mu_2\gamma_1 & -\mu_1\gamma_1 & 0 \end{pmatrix},$$

where $\gamma_1 = T_{Xd}/m$, $\gamma_2 = \gamma_1 + (g - \mu_3)$. From (9), γ_1 and γ_2 are positive and bounded if $\boldsymbol{F}$ is bounded. With simple derivation, we obtain the following formulation:

$$\begin{aligned} \dot{\gamma}_1 &= \frac{1}{\gamma_1}\begin{pmatrix}\mu_1 & \mu_2 & -(g-\mu_3)\end{pmatrix}\dot{\boldsymbol{F}}, \\ \dot{\gamma}_2 &= \dot{\gamma}_1 - \dot{\mu}_3. \end{aligned}$$

From the formulation, it is clear that γ_1, γ_2, $\dot{\gamma}_1$ and $\dot{\gamma}_2$ are all bounded when $\boldsymbol{F}$ and $\dot{\boldsymbol{F}}$ are bounded. And under this situation, as a function of $\boldsymbol{F}$, $\dot{\boldsymbol{F}}$, $\dot{\gamma}_1$ and $\dot{\gamma}_2$, $\dot{\boldsymbol{\Xi}}(\boldsymbol{F})$ is also bounded. From (10) and (11) it is concluded that $\boldsymbol{\omega}_d$ and $\dot{\boldsymbol{\omega}}_d$ are both bounded if $\boldsymbol{F}$, $\dot{\boldsymbol{F}}$ and $\ddot{\boldsymbol{F}}$ are bounded.

By using the intermediary control law (20), we obtain the following formulation:

$$\begin{aligned} \boldsymbol{F} &= \ddot{\boldsymbol{p}}_d - \hat{\boldsymbol{\sigma}}_2\left(\dot{\bar{\boldsymbol{p}}} + \hat{\boldsymbol{\sigma}}_1(\bar{\boldsymbol{p}})\right), \\ \dot{\boldsymbol{F}} &= \boldsymbol{p}_d^{(3)} - \dot{\hat{\boldsymbol{\sigma}}}_2\left(\dot{\bar{\boldsymbol{p}}} + \hat{\boldsymbol{\sigma}}_1(\bar{\boldsymbol{p}})\right)\cdot\left(\ddot{\bar{\boldsymbol{p}}} + \dot{\hat{\boldsymbol{\sigma}}}_1(\bar{\boldsymbol{p}})\dot{\bar{\boldsymbol{p}}}\right) \\ &= \boldsymbol{p}_d^{(3)} - \dot{\hat{\boldsymbol{\sigma}}}_2\left(\bar{\boldsymbol{v}} + \hat{\boldsymbol{\sigma}}_1(\bar{\boldsymbol{p}})\right)\cdot\big(g\hat{\boldsymbol{e}}_3 - \gamma_1\boldsymbol{R}(\boldsymbol{Q})^T\hat{\boldsymbol{e}}_{3b} \\ &\quad -\ddot{\boldsymbol{p}}_d + \dot{\hat{\boldsymbol{\sigma}}}_1(\bar{\boldsymbol{p}})\bar{\boldsymbol{v}}\big), \\ \ddot{\boldsymbol{F}} &= \boldsymbol{p}_d^{(4)} - \ddot{\hat{\boldsymbol{\sigma}}}_2\left(\dot{\bar{\boldsymbol{p}}} + \hat{\boldsymbol{\sigma}}_1(\bar{\boldsymbol{p}})\right)\cdot\left(\ddot{\bar{\boldsymbol{p}}} + \dot{\hat{\boldsymbol{\sigma}}}_1(\bar{\boldsymbol{p}})\dot{\bar{\boldsymbol{p}}}\right)^2 \\ &\quad -\dot{\hat{\boldsymbol{\sigma}}}_2\left(\dot{\bar{\boldsymbol{p}}} + \hat{\boldsymbol{\sigma}}_1(\bar{\boldsymbol{p}})\right)\cdot\left(\dddot{\bar{\boldsymbol{p}}} + \ddot{\hat{\boldsymbol{\sigma}}}_1(\bar{\boldsymbol{p}})\left(\dot{\bar{\boldsymbol{p}}}\right)^2 + \dot{\hat{\boldsymbol{\sigma}}}_1(\bar{\boldsymbol{p}})\ddot{\bar{\boldsymbol{p}}}\right) \\ &= \boldsymbol{p}_d^{(4)} - \ddot{\hat{\boldsymbol{\sigma}}}_2\left(\bar{\boldsymbol{v}} + \hat{\boldsymbol{\sigma}}_1(\bar{\boldsymbol{p}})\right)\cdot\big(g\hat{\boldsymbol{e}}_3 - \gamma_1\boldsymbol{R}(\boldsymbol{Q})^T\hat{\boldsymbol{e}}_{3b} \\ &\quad -\ddot{\boldsymbol{p}}_d + \dot{\hat{\boldsymbol{\sigma}}}_1(\bar{\boldsymbol{p}})\bar{\boldsymbol{v}}\big)^2 - \dot{\hat{\boldsymbol{\sigma}}}_2\left(\bar{\boldsymbol{v}} + \hat{\boldsymbol{\sigma}}_1(\bar{\boldsymbol{p}})\right) \\ &\quad \cdot\big(\dot{\gamma}_1\boldsymbol{R}(\boldsymbol{Q})^T\hat{\boldsymbol{e}}_{3b} + \gamma_1\boldsymbol{R}(\boldsymbol{Q})^T\boldsymbol{S}(\boldsymbol{\omega})\hat{\boldsymbol{e}}_{3b} - \boldsymbol{p}_d^{(3)} \\ &\quad +\ddot{\hat{\boldsymbol{\sigma}}}_1(\bar{\boldsymbol{p}})\bar{\boldsymbol{v}}^2 + \dot{\hat{\boldsymbol{\sigma}}}_1(\bar{\boldsymbol{p}})\ddot{\bar{\boldsymbol{p}}}\big). \end{aligned}$$

Under *Assumption* 4 the desired trajectory $\boldsymbol{p}_d$ and its derivatives are all bounded, and from (18) the saturation functions $\hat{\boldsymbol{\sigma}}_i(\cdot)$, $i = 1, 2$ are also bounded. It should be noted that the error function $f(\boldsymbol{Q}, \boldsymbol{Q}_d)$ is always bounded, no matter whether the attitude error $\bar{\boldsymbol{q}}$ is asymptotically stable. So according to Theorem 1, it is concluded that the states $(\bar{\boldsymbol{p}}, \bar{\boldsymbol{v}})$ are bounded. And by substituting (20) into (7), we can obtain the following formulation:

$$\ddot{\bar{\boldsymbol{p}}} = -\hat{\boldsymbol{\sigma}}_2\left(\dot{\bar{\boldsymbol{p}}} + \sigma_1(\bar{\boldsymbol{p}})\right) + f(\boldsymbol{Q}, \boldsymbol{Q}_d).$$

It is clear that $\ddot{\bar{\boldsymbol{p}}}$ is also bounded. Because of the boundedness of $\boldsymbol{p}_d^{(n)}$, $n = 1, 2, 3, 4$, $\hat{\boldsymbol{\sigma}}_i$, $i = 1, 2$, $\bar{\boldsymbol{v}}$ and $\ddot{\bar{\boldsymbol{p}}}$, we can draw the conclusion that $\boldsymbol{F}$, $\dot{\boldsymbol{F}}$ and $\ddot{\boldsymbol{F}}$ are all bounded,

which leads to the boundedness of angular velocity $\boldsymbol{\omega}_d$ and angular acceleration $\dot{\boldsymbol{\omega}}_d$.

REFERENCES

[1] N. Knoebel, S. Osborne, D. Snyder, T. Mclain, R. Beard, and A. Eldredge, "Preliminary modeling, control, and trajectory design for miniature autonomous tailsitters," in *Proc. AIAA Guid., Navigat., Control Conf. Exhib.*, 2006, p. 6713.
[2] R. H. Stone, P. Anderson, C. Hutchison, A. Tsai, P. Gibbens, and K. C. Wong, "Flight testing of the t-wing tail-sitter unmanned air vehicle," *J. Aircr.*, vol. 45, no. 2, pp. 673–685, Mar/Apr. 2018.
[3] M. Aksugur, G. Inalhan, and R. Beard, "Hybrid propulsion system design of a VTOL tailsitter UAV," SAE Technical Paper 2008-01-2242, 2008.
[4] Y. Jung and D. H. Shim, "Development and application of controller for transition flight of tail-sitter UAV," *J. Intell. Robotic Syst.*, vol. 65, nos. 1–4, pp. 137–152, 2012.
[5] Y. Jung, S. Cho, and D. H. Shim, "A comprehensive flight control design and experiment of a tail-sitter UAV," in *Proc. AIAA Guid., Navigat., Control (GNC) Conf.*, 2013, p. 4992.
[6] X. Yang, L. Dong, W. Liaoni, and S. Yangyang, "Design and implementation of twin-rotor tail-sitter UAV," in *Proc. IEEE Adv. Inf. Technol. Electron. Automat. Control Conf. (IAEAC)*, Dec. 2015, pp. 406–410.
[7] C. Zhang, J. Zhu, K. Liu, X. Yuan, and Y. Gao, "Model and longitudinal hover control of a conceptual thrust-vectored unmanned tail-sitter," in *Proc. 10th IEEE Int. Conf. Control Automat. (ICCA)*, Jun. 2013, pp. 1714–1717.
[8] A. Ailon, "Simple tracking controllers for autonomous VTOL aircraft with bounded inputs," *IEEE Trans. Autom. Control*, vol. 55, no. 3, pp. 737–743, Mar. 2010.
[9] A. Hably and N. Marchand, "Global stabilization of a four rotor helicopter with bounded inputs," in *Proc. IEEE Int. Conf. Intell. Robots Syst. (IROS)*, Oct. 2007, pp. 129–134.
[10] I. A. Raptis, K. P. Valavanis, and W. A. Moreno, "A novel nonlinear backstepping controller design for helicopters using the rotation matrix," *IEEE Trans. Control Syst. Technol.*, vol. 19, no. 2, pp. 465–473, Mar. 2011.
[11] J. F. Guerrero-Castellanos, N. Marchand, A. Hably, S. Lesecq, and J. Delamare, "Bounded attitude control of rigid bodies: Real-time experimentation to a quadrotor mini-helicopter," *Control Eng. Pract.*, vol. 19, no. 8, pp. 790–797, Aug. 2011.
[12] M.-D. Hua, T. Hamel, P. Morin, and C. Samson, "A control approach for thrust-propelled underactuated vehicles and its application to VTOL drones," *IEEE Trans. Autom. Control*, vol. 54, no. 8, pp. 1837–1853, Aug. 2009.
[13] C.-T. Lee and C.-C. Tsai, "Adaptive backstepping integral control of a small scale helicopter for airdrop missions," *Asian J. Control*, vol. 12, no. 4, pp. 531–541, 2010.
[14] J. Hu and H. Zhang, "Immersion and invariance based command-filtered adaptive backstepping control of VTOL vehicles," *Automatica*, vol. 49, no. 7, pp. 2160–2167, 2013.
[15] J. Hu and H. Zhang, "Globally asymptotically stable saturated PID controllers for a double integrator with constant disturbance," *Int. J. Robust Nonlinear Control*, vol. 24, no. 10, pp. 1488–1504, 2014.
[16] S. Gayaka, L. Lu, and B. Yao, "Global stabilization of a chain of integrators with input saturation and disturbances: A new approach," *Automatica*, vol. 48, no. 7, pp. 1389–1396, 2012.
[17] Z. Zhu, Y. Xia, and M. Fu, "Adaptive sliding mode control for attitude stabilization with actuator saturation," *IEEE Trans. Ind. Electron.*, vol. 58, no. 10, pp. 4898–4907, Oct. 2011.
[18] A.-M. Zou, K. D. Kumar, and A. H. J. de Ruiter, "Robust attitude tracking control of spacecraft under control input magnitude and rate saturations," *Int. J. Robust Nonlinear Control*, vol. 26, no. 4, pp. 799–815, 2015.
[19] A.-M. Zou and K. D. Kumar, "Adaptive fuzzy fault-tolerant attitude control of spacecraft," *Control Eng. Pract.*, vol. 19, no. 1, pp. 10–21, 2011.
[20] J. D. Boškovic, S.-M. Li, and R. K. Mehra, "Robust adaptive variable structure control of spacecraft under control input saturation," *J. Guid., Control, Dyn.*, vol. 24, no. 1, pp. 14–22, 2001.
[21] J. D. Boskovic, S.-M. Li, and R. K. Mehra, "Robust tracking control design for spacecraft under control input saturation," *J. Guid., Control, Dyn.*, vol. 27, no. 4, pp. 627–633, 2004.
[22] M. D. Hua, T. Hamel, P. Morin, and C. Samson, "Control of thrust-propelled underactuated vehicles," Institut National de Recherche en Informatique et Automatique, Tech. Rep. 6453, 2008.
[23] J. M. Pflimlin, P. Souères, and T. Hamel, "Position control of a ducted fan VTOL UAV in crosswind," *Int. J. Control*, vol. 80, no. 5, pp. 666–683, 2007.
[24] A. Roberts and A. Tayebi, "Adaptive position tracking of VTOL UAVs," *IEEE Trans. Robot.*, vol. 27, no. 1, pp. 129–142, Feb. 2011.
[25] A. Abdessameud and A. Tayebi, "Global trajectory tracking control of VTOL-UAVs without linear velocity measurements," *Automatica*, vol. 46, no. 6, pp. 1053–1059, 2010.
[26] N. B. Knoebel and T. W. McLain, "Adaptive quaternion control of a miniature tailsitter UAV," in *Proc. Amer. Control Conf.*, 2008, pp. 2340–2345.
[27] M. E. Argyle, J. M. Beach, R. W. Beard, T. W. McLain, and S. Morris, "Quaternion based attitude error for a tailsitter in hover flight," in *Proc. Amer. Control Conf.*, 2014, pp. 1396–1401.
[28] J. M. Beach, M. E. Argyle, T. W. McLain, R. W. Beard, and S. Morris, "Tailsitter attitude control using resolved tilt-twist," in *Proc. Int. Conf. Unmanned Aircr. Syst. (ICUAS)*, 2014, pp. 768–779.
[29] Y. Jiali and Z. Jihong, "Dynamic modelling of a small scale turbojet engine," in *Proc. IEEE Eur. Control Conf.*, Jul. 2015, pp. 2750–2755.
[30] M. Euston, P. Coote, R. Mahony, J. Kim, and T. Hamel, "A complementary filter for attitude estimation of a fixed-wing UAV," in *Proc. IEEE/RSJ Int. Conf. Intell. Robots Syst.*, Sep. 2008, pp. 340–345.

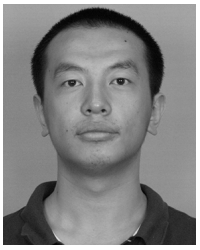

LINFENG WU received the bachelor's degree in control science and engineering from Tsinghua University, Beijing, China, in 2013, where he is currently pursuing the Ph.D. degree with the Department of Automation. His research interests include flight control for VTOL UAVs and nonlinear control.

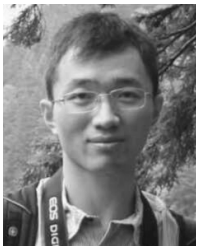

HUANYU LI received the bachelor's degree in electronic engineering and the Ph.D. degree in control science and engineering from Tsinghua University, China, in 2012 and 2017, respectively. His research interests include data fusion and flight control for VTOL UAVs.

YINGJIE LI received the bachelor's degree in flight vehicle propulsion engineering from Beihang University, China, in 2007 and the master's degree in electrical engineering from Tsinghua University, Beijing, China, in 2011, where he is currently pursuing the Ph.D. degree with the Department of Automation. His research interests include flight vehicle propulsion systems and thrust-vectoring control for VTOL UAVs.

CHUNWEN LI received the bachelor's and Ph.D. degrees in control science and engineering from Tsinghua University, Beijing, China, in 1982 and 1989, respectively, where he is currently a Professor with the Department of Automation. His research interests include nonlinear control and inverse system control.